Influence of CO_2 Injection on Biomass Gasification

Heidi C. Butterman and Marco J. Castaldi*

Department of Earth & Environmental Engineering (HKSM), Columbia University, New York, New York 10027

The impact of CO_2 cofeed (0−50% by volume) on steam gasification of biomass was investigated via thermogravimetric analysis−gas chromatography (TGA-GC). H_2, CO_2, CO, and CH_4 gas evolution as a function of temperature were quantified for various S/C and CO_2/C ratios. CO evolution enhancement became significant at temperatures above 700 °C for all woods and grasses studied. H_2 evolution began at temperatures above 450 °C and began to decline above 700 °C. All samples had similar mass decay curves that were completed by 900−1000 °C and were independent of the amount of CO_2 injection. Improved char conversion was observed when CO_2 was present. The biomass fuels and their ash residue were analyzed using atomic absorption spectroscopy (AAS) and scanning electron microscopy/energy dispersive X-ray analysis (SEM/EDX). A significant amount of highly corrosive ash residues were observed with no CO_2, yet much smaller volumes were observed when CO_2 was present. Finally, the experimental data was compared to ASPEN simulations to understand the influence of CO_2 recycle for carbon based fuels, and they showed good agreement.

1. Introduction

The need to meet increasing energy demands, while addressing the importance of energy security and environmental impact, has resulted in renewed interest in alternatives to fossil fuels. Biomass constitutes one of the more promising carbon neutral energy sources that can be part of the solution. Since biomass fuels are globally available and do not have the intermittency associated with wind and photovoltaics, and they constitute nearly one-quarter of the fuel available from municipal solid waste, the thermal processing of biomass offers the potential to transition from a fossil fuel driven global economy.[1]

Biomass fuels currently provide 3% of the U. S. energy production, yet nearly one-third of the renewable energy sources in the United States can be attributed to woods, grasses, and agricultural forestry wastes and residues.[2] On the basis of a recent study, biomass has the capacity for supplying 5% of the nation's power by 2030, and biomass-derived fuels have the potential to provide 20% of the U. S. transportation demand.[3] With energy consumption expected to double over the next 40 years and with heightened environmental consciousness as to the need for limiting CO_2 atmospheric emissions, the feasibility of biomass-derived fuels as one of the significant carbon neutral energy solutions has emerged. Making fuels from biomass typically entails thermal treatment.

The thermal treatment of plant-derived fuels can be by either pyrolysis, gasification, or combustion. The complex lignocellulosic structure of biomass renders it more difficult to either gasify or combust. Direct combustion of biomass feedstocks results in fuel-bound nitrogen and sulfur being converted to NO_x and SO_x. Gasification offers the opportunity to control the level of gaseous and particulate emissions, leading to lower concentrations of soot particles, aerosols, NO_x, and SO_x and the production of clean fuel gas or chemical feedstock streams (e.g., H_2, CO, or CH_4). Much of the mass decay during biomass decomposition occurs at lower pyrolysis temperatures. The steam-gasification process enables thermal treatment under a reducing atmosphere that leads to fuel-bound nitrogen release as N_2 and fuel-bound sulfur conversion to H_2S that is more easily removed by means of adsorption beds. Furthermore, introduction of steam in the feed can be used to enhance the H_2 production during the gasification process. There have been numerous studies demonstrating the enhanced H_2 production from carbon based fuels through the use of steam in the gasifying medium. Most of these studies have investigated gaseous evolution from thermal treatment of coal, though several have been in-depth studies of the gasification products for other fuels such as municipal solid waste and biomass.[12−14]

Other reforming enhancements, such as adsorption-enhanced reforming (AER) in which the CO_2 is removed to push the equilibrium forward in the water gas shift (WGS) reaction,

$$CO + H_2O \rightarrow H_2 + CO_2 \qquad \Delta H = -41.2 \text{ kJ/mol} \quad (1)$$

are effective strategies to increase hydrogen concentration during steam gasification. Several studies have involved the use of H_2, O_2, Ar, He, air, CO, and CO_2 or a combination of these along with steam to enhance the gasification of the carbon based fuels. Of the several experimental investigations that have been done to study the nature of enhanced steam gasification of biomass feedstocks with CO_2, none have involved an in-depth study of the specific influence of CO_2 concentration on each of the gas species evolved. Presented below are the studies done that are closest to the present work having elements relevant to those in the current investigation.

Iyer et al.[4] studied the gas evolution from adsorption-enhanced steam reforming (AER) of syngas during coal gasification. Their "calcium looping" scheme involved CO_2 and H_2S adsorption onto a reactive proprietary mesoporous precipitated calcium carbonate sorbent (PCC) at high steam-gasification temperatures (700−900 °C). Continuous CO_2 removal resulted in lower CO levels and higher H_2 concentrations. Without regeneration of the sorbent, the higher CO_2 levels led to a reverse WGS reaction with lower H_2 concentration and higher CO concentration. In another study,[5] they observed that the level of CO_2 began to rapidly rise with decreasing adsorption for temperatures 650 and 700 °C and pressures of 1, 10, and 20 atm. This coincided with a rapid drop in the level of CO conversion. This resulted in a corresponding steep decline for all of the H_2 concentration curves as the CO levels abruptly increased.

Bretado et al.[6] performed a thermodynamic analysis for the adsorption-enhanced production of H_2 using a Na_2ZrO_3 adsorbent. A rapid rise in CO_2 levels corresponded to a rise in CO

* Corresponding author. E-mail: mc2352@columbia.edu. Tel.: (212) 854-6390. Fax: (212) 854-7081.

10.1021/ie071160n CCC: $37.00
Published on Web 11/28/2007

and Na_2ZrO_3 and a sharp drop in ZrO_2 and H_2 in the temperature range 600−700 °C. Specht et al.[7] performed a set of thermodynamic equilibrium calculations for the H_2 generation from CH_4 using an adsorption-enhanced reforming (AER) process at atmospheric pressure, with 2.5 mol of steam and 1 mol each of CH_4 and CaO. Desorption of CO_2 from $CaCO_3$ to regenerate the CaO was observed at 700 °C, with a corresponding increase in CO and a decrease in H_2 with increasing CO_2 levels.

Alma et al.[8] studied AER in a batch reactor and analyzed gas evolution from cellulose, switchgrass, willow, and deinking sludge. As a result of decreased levels of CO_2 in the reactor due to increased adsorption by CaO, they observed the total H_2 gas yield at 650 °C to increase in the batch reactor. This trend in enhanced H_2 production via AER steam gasification of "woody biomass" was also observed at 5 and 10 atm. Pfeifer et al.[9] studied the steam gasification of wood chips and pellets using fast internally circulating fluidized-bed (FICFB) technology. They used a calcite adsorbent to selectively remove CO_2 for transport from the gasification (600−700 °C) to the combustion (800−900 °C) zone; they were able to increase H_2 yield from 35 to 40% without AER to between 66 and 75% with AER. The CO_2 produced by biomass gasification in the first fluidized bed was sent to the second bed to enhance the residual biomass char combustion.

Mollenstedt et al.[10] studied the adsorption-enhanced steam gasification of wood. They used dolomite and calcite adsorbents to remove the CO_2 from their fluidized-bed gasifier at 650 °C and atmospheric pressure, shifting via WGS the equilibrium from CO toward H_2. The CO_2 adsorption results in a product gas of high H_2 concentration and provides the heat necessary for the endothermic reactions in the gasifier. While CH_4 levels remained very low and nearly constant, the product gas concentrations of H_2 decreased and CO increased as the CO_2 concentration rose. Eventually, the adsorbent became saturated, and CO_2 breakthrough resulted in high CO_2 concentrations corresponding to high CO concentrations, decreased H_2 production, and continuous low levels of CH_4 for bed temperatures of ∼650 °C. The product gas composition during the adsorption-enhanced steam gasification of wood pellets showed continuously oscillating low CH_4 concentrations. This correlated with increasing levels of CO and tar and decreasing levels of H_2 with increasing CO_2 levels for gasification/adsorption occurring at 640 °C and combustion/desorption occurring at 830 °C.

Song[11] proposed the concept of CO-enriched gasification (COEG) for production of H_2 from steam gasification of coal and biomass. Recycling a portion of CO_2 taken from an inline (PSA) absorber back into the gasifier enhances CO formation through the Boudouard reaction. Nehrozoglu[12] designed a new integrated gasification combined cycle (IGCC) plant configuration that recycles the CO_2, H_2O, and any excess oxygen from the gas turbine exhaust back to the circulating fluidized bed (CFB) where pulverized coal undergoes steam gasification. The recycle of high temperature, high-pressure CO_2 results in lower cost, higher system efficiency, and more complete steam gasification of the pulverized coal.

Senneca[13] performed a series of pyrolysis, char-combustion, and gasification experiments on pine seed shells, olive husk, and wood chips. The aim was to study the intrinsic reactivity, the mass decay under different heating rates, the pore structure of the char, and the influence of heating rate and gasifying medium (H_2O, CO_2, N_2, $5\%O_2-N_2$) for temperatures between 100−900 °C. Olive husks were the most reactive and exhibited the highest char gasification rates in CO_2, while wood chips had the lowest CO_2 gasification rates. The high reactivity of olive husks was attributed to its mineral content with potassium oxide in the ratio of 26:5:1 for olive husks, pine seed shells, and wood chips, respectively. The char gasification rate in steam was found to be dependent upon the degree of carbon conversion. Steam gasification with CO_2 was observed to enhance the microporous structure but not to encourage the growth of macropores.

Minkova et al.[14] investigated the pyrolysis and gasification of biomass in H_2O, Ar, and CO_2-H_2O environments at atmospheric pressure under a slow heating rate of 10 °C/min from ambient to 750 °C with a 2 h peak temperature hold in the reactor. The presence of both steam and CO_2 as reactive agents was seen to decrease the yield of solid residue. The CO_2-H_2O gasification environment was found to be most conducive to char activation with enhanced pore structure and surface area development. These are similar findings to those of Ye et al.[15] The oxygen functional groups were mostly acidic in character when oxidation occurred above 200 °C, though they were mostly basic when oxidation occurred above 500 °C. Activated carbons produced by CO_2-H_2O gasification had greater amounts of basic and weakly acidic oxygenated groups. Biomass samples having predominantly basic groups were found to exhibit better thermal resistance. These high-temperature chars are a direct consequence of the reactive medium, CO_2-H_2O, in which they were formed.

Demirbas[16] has done extensive experimental studies of biomass char structure and characterization, as well as the mechanistic development necessary to explain biomass degradation and char development. They found that chars from hazelnut shell and wheat straw were more reactive than those from oak wood due to their higher ash content. Investigating the chars resulting from steam gasification between 950−1250 K, they observed greater char yields in the higher lignin content biomass such as hazelnut shells as compared to the lower lignin oak wood and wheat straw.

Orfao et al.[17] developed a model for the pyrolysis kinetics of lignocellulosic material. The three-part model corresponded to the three biomass structural components: Avicel cellulose, Sigma xylan for hemicellulose, and Westvaco pine wood lignin. Differential thermogravimetry (DTG) curves for the "representative" lignocellulosic materials showed that lignin starts to decompose at the lowest temperature ∼110 °C, though its rate is so slow and spread over such a large temperature range to ∼900 °C. Therefore, the char resulting from biomass pyrolysis is mainly due to the lignin content of the lignocellulosic material, though the xylan, representing the hemicellulose component, plays a measurable role in the formation of pyrolysis chars.

Babu and Chaurasia[18] designed a model that simulated the chemical processes occurring in their downdraft biomass gasifier using the moisture content as a key process parameter for gas-evolution comparison. They chose char reactivity, which was observed to be dependent on the number of active sites on the microporous char structure, as a key modeling parameter. The gasifier model of Sheth and Babu[19] predicted initially decreasing levels of CO_2 along the gasifier bed that corresponded to decreasing CO levels. Simultaneously, the H_2 mole fraction on a dry basis predicted increasing values for a given moisture content, bed length, incoming flow velocity, and initial temperature of 1400 K at atmospheric pressure.

Through a multiple regression analysis, Sears et al.[20] developed a reaction rate expression for the kinetics of the coal char−CO_2 gasification reaction in terms of the intrinsic carbon activity. The char kinetic reaction rate was found to depend upon oxygen levels inherent in the char as well as catalytically controlled

char−CO_2 enhanced adsorption that determined the rate of delivery of surface O for char burnout.

Ochoa et al.[21] studied the CO_2 gasification kinetics of subbituminous (SB) and high-volatile bituminous (HVB) coal chars. The char reactivities for CO_2 concentrations of 50−70% at temperatures between 900−1150 °C were shown to be functions of the carbon content, mineral content, crystallinity, and microporosity. CO_2 enhanced gasification of the chars was observed to be kinetically controlled for temperatures below 1150 °C, whereas the rate of CO_2 gasification was observed to be diffusion limited at higher temperatures for the 50−70% CO_2 concentrations examined for both types of low-rank, high-moisture coals.

Ye et al.[15] investigated the gasification of a low-rank Bowmans coal using steam and CO_2. For temperatures between 714−892 °C at atmospheric pressure, the gasification reactions were all kinetic controlled. CO_2−steam-gasification reactivities for acid-washed Bowmans coal, in which all alkali and alkaline earth and all metal compounds that were not acid-insoluble had been removed, were similar to the reactivity of low-mineral coal. CO_2 enhanced gasification of the coal chars was found to be via catalytic effects, where the catalysts had to be chemically bound to the functional groups, not just physically associated with the char surface.

Messenbock et al.[22] examined the combustion reactivities of Daw Mill coal char at 1000 °C and found a rapid drop in CO_2−char reactivity to low stable values due to tar repolymerization. Enhanced char burnout with CO_2 affects the char reactivity by facilitating the burnout of the unreactive layer and by changing the pore structure and increasing the extent of the microporous network as evidenced in their scanning electron microscopy (SEM) micrographs.

The feasibility of recycling CO_2 to enhance the gasification process of carbon based fuels was investigated by Castaldi and Dooher[23] using an ASPEN thermodynamic simulation to model the gaseous evolution and energy output. The ASPEN calculations indicated that the enhanced CO levels and decreased energy requirements were most probably due to acceleration of the slightly exothermic water gas shift reaction coupled with the gasification attributable to the highly endothermic Boudouard reaction. The discussion above highlights related research that did not investigate product gas species evolution from biomass samples as a function of temperature introducing CO_2 into the steam-gasification process.

The dominant reactions driving biomass steam gasification in the 700−1200 °C range are the steam reforming reaction

$$C + H_2O \rightarrow CO + H_2 \qquad \Delta H = +131.3 \text{ kJ/mol} \quad (2)$$

and the Boudouard reaction

$$C + CO_2 \rightarrow 2CO \qquad \Delta H = +172.5 \text{ kJ/mol} \quad (3)$$

in addition to the reactions cleaving and condensing the biomass lattice structure during pyrolysis, the decomposition reactions of the oxygenated minerals releasing O_2, and the oxidation of the char

$$C + {}^1/_2O_2 \text{ (from biomass structure)} \rightarrow CO \qquad \Delta H = -110.5 \text{ kJ/mol} \quad (4)$$

to release CO and CO_2 as the char degrades from a hydrocarbon skeleton to a mineral ash residue as well as the reverse water gas shift reaction.

$$H_2 + CO_2 \rightarrow CO + H_2O \qquad \Delta H = +41.2 \text{ kJ/mol} \quad (5)$$

Optimum methane production appeared to occur in the interval 500−600 °C. Not until about 700 °C could a pronounced depression in the H_2 concentration be discerned. A distinct enhancement of CO evolution with CO_2 recycle and a pronounced increase in CO concentration due to the Boudouard reaction was the strongest signal in the gasification process. Pyrolysis of biomass up to ∼450 °C can result in significant quantities of tar and char that, through subsequent thermal treatment at elevated temperatures, can yield enhanced production of gaseous products.

While an industrial process might use the offgas stream containing CO_2 with some H_2, CO, and other hydrocarbons for recycle back into the gasification zone, our use of CO_2 with only a N_2 inert gas was used to try to understand the specific influence of CO_2 on enhanced char burnout with more complete conversion at elevated temperatures during the steam gasification of biomass. Though the present investigation focused on CO_2 in a N_2 diluent, it is likely that the CO_2 in a commercial plant would be obtained from combustion or gasification recycle flows. These process flows would probably contain H_2, CO, and H_2O that could influence the distribution of gasification products.

Using CO_2 as a coreactant can enhance the char burnout rates that will result in either increased throughputs or the need for smaller units. Additionally, the injection of CO_2 and H_2O increases the char reactivity that results in more efficient use of the feedstock with less residual to be postprocessed. As an application of the findings from the present study for CO_2 enhanced steam gasification, a promising design improvement might involve the CO_2 injected strategically in locations within the gasifier where char formation levels are highest.

Biomass chemical composition is highly variable, and this leads to a correspondingly wide range in heat content and characteristic species evolution from the various feedstocks. Use of the thermogravimetric analyzer and the gas chromatograph along with a knowledge of the distribution of lignocellulosic components enables us to study gaseous evolution as a function of composition, mass loss, and temperature. We can then select the more likely clusters of coupled reactions and reaction pathways responsible for the gas concentrations that we are observing in the effluent as well as the influence that CO_2 plays in the steam-gasification process. Further credibility for the catalytic gasification concept of Castaldi and Dooher[23] came from experimental confirmation of the ASPEN numerical simulations. The numerical model was for the thermal treatment of a carbon fuel with enhanced gasification due to CO_2 recycle. Simulation results correlated well with similar experimental trends observed in the actual biomass gasification with CO_2 and H_2O fed into the line.

2. Experimental Setup

2.1. Gasification System. Figure 1 shows a schematic diagram of the gasification test facility in the Combustion and Catalysis Laboratory at Columbia University. It consists of a Dupont 990 thermal analyzer that can regulate the temperature and heating rate of the quartz furnace in the Dupont 950 thermogravimetric analyzer. UHP N_2 and Bone Dry CO_2 cylinders feed gases whose flow rates are regulated by means of two Gilmont GF 1060 rotameters.

Distilled water regulated by a kd-Scientific 780-100 syringe pump is fed into a stainless steel steam generator. Slightly superheated (∼110−120 °C) steam is produced whose temper-

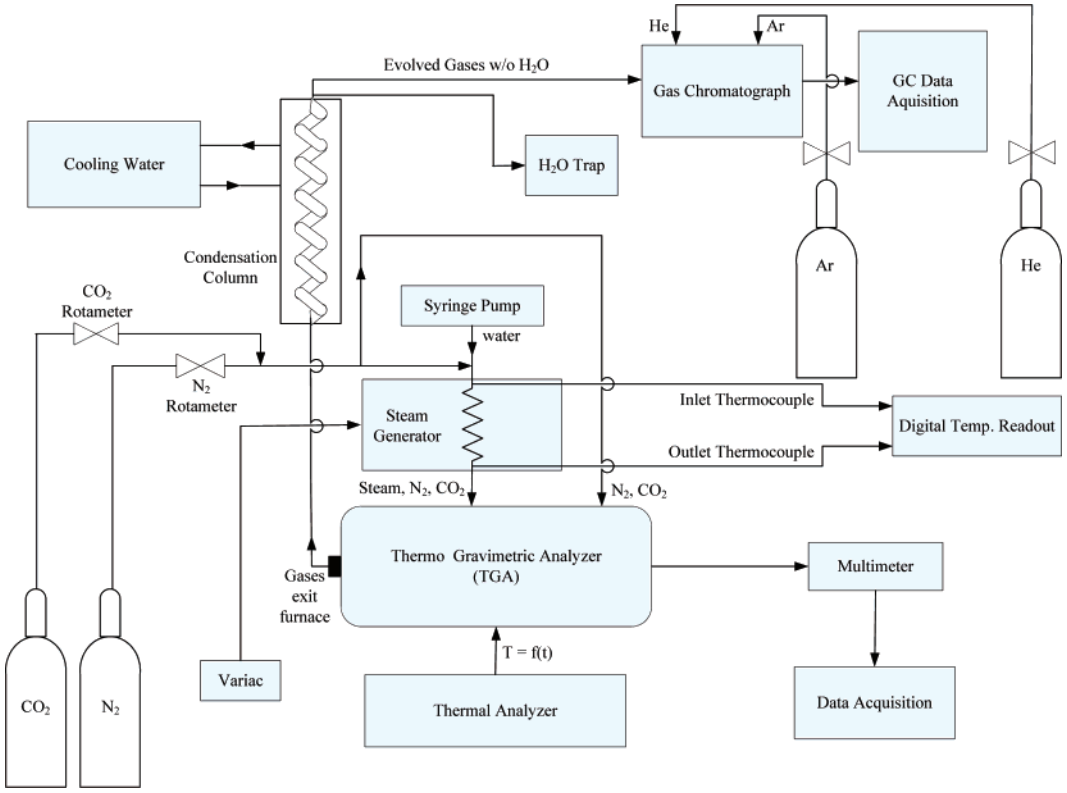

Figure 1. Schematic of experimental apparatus.

ature is monitored by an Omega digital E-type thermocouple readout as it joins the CO_2 and N_2 line flow into the furnace. This stream combines with the N_2 carrier gas entering the furnace and prevents any backflow of gasification residue that could lead to deposition on the thermogravimetric analysis (TGA) electronics. Our steam-to-carbon ratios varied from 5.5 to 48, on a molar basis, and the volume % of CO_2 fed into the line ranged from 0 to 50%. The molar flow rate of CO_2 is calculated from the volumetric % CO_2 and the constant total feed flow of 90 mL/min. The molar flow rate of steam was set by the syringe pump. This was based on the saturation value into the steam generator to ensure that the H_2O entered the line flow as gaseous steam. The molar rate of biomass C is estimated from the slope of the mass decay curve for a given feedstock whose value appeared to be independent of the specific volume % CO_2 fed into the line. Calculation of the gasification slope is at 750 °C, which was judged to be an appropriate gasification temperature for evaluating the average burnout of the carbon char structure. We were running the process with excess H_2O and CO_2 to ensure that the biomass was the limiting agent in the gasification reactions. The biomass sample sits inside the furnace on an inert pan suspended from either a quartz or ceramic rod. The ceramic alternative was a recent response to the repeated destruction of the thin quartz support rods due to embrittlement. Mass and temperature change of the TGA sample are recorded by a Keithley 2701 multimeter, and data acquisition is accomplished by means of Keithley ExcelLINX software. Gasification products exit the furnace and pass through an ice−water trap system that removes any moisture from the evolved gases before entering the Agilent 3000A micro-gas chromatograph. UHP He and UHP Ar cylinders provide the carrier gas for the 4-channel micro-GC. The resulting sensitivity of the instrument is in the single-digit ppmV range with single-digit ppmV resolution. The GC data is processed by means of Agilent Cerity software.

2.2. Methodology of Gasification Testing. Biomass samples were prepared by drilling cores in untreated wood planks to produce fine sawdust or they were dried, ground by mortar and pestle, and then ball-milled. The bark, needles, and grasses were air-dried and subjected to grinding by mild processing to minimize the degradation of the chemical structure since dried pine needles and green pine needles did not exhibit identical gas evolution profiles. The grasses were not washed in water since this could remove some of the mineral content, but they were cleaned of debris and all sand grains were carefully removed from the American beachgrass.

Feedstocks that were studied include Douglas fir, white pine, spruce, poplar, sugar maple, oak, alfalfa, cordgrass, American beachgrass, pine bark, maple bark, dried pine needles, green pine needles, and cotton plant. Samples were typically 20−25 mg. For the present study, a wider range in sample mass was used to investigate gas evolution over a greater range of S/C and CO_2/C ratios. The poplar sample was 25 mg, Douglas fir was 16 mg, beachgrass was 34 mg, and the large pan beachgrass sample had a mass of 110 mg. These samples were weighed on a Mettler balance accurate to the nearest ±0.1 mg.

The total line feed as measured by the syringe pump and the two rotameters was set to the desired CO_2 concentration so that the total feed flow rate (steam + CO_2 + N_2) remained constant at 90 mL/min. Bone dry CO_2, UHP N_2, and distilled water flowed through the line into the furnace. The small mass of the sample and the relatively large feed volumes due to the CO_2 and N_2 resulted in significant dilution of the evolved gases introduced into the micro-GC. UHP Ar was used as the carrier gas to detect H_2, CO, and CH_4 on channel 1, which uses a molecular sieve column. UHP He was used as the carrier gas for the other three channels of the GC. Channel 2 uses a porous layer open tubular PLOT-U column by which CO_2 concentrations are detected. The temperature was ramped by the thermal analyzer at a constant 10 °C/min from ambient to a thermo-

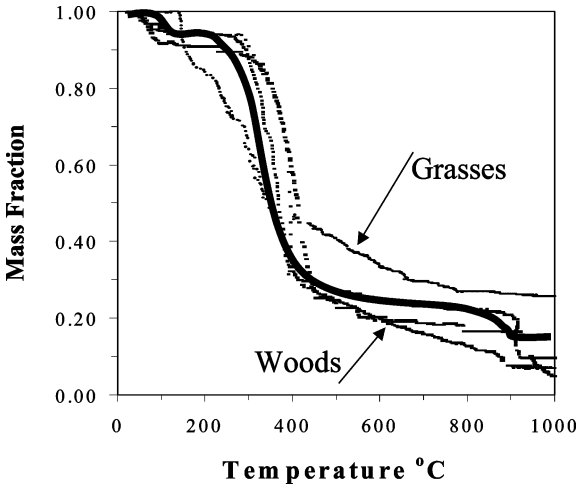

Figure 2. Mass decomposition curve for representative biomass samples, $CO_2/C = 0$, S/C varies from 17 to 48.

couple corrected temperature of 1000 °C. The Keithley monitored temperature and mass changes every 10 s, and the GC was synchronized to sample the gases exiting the furnace approximately every 4 min.

3. Results and Discussion

3.1. Physical Observations. Thermogravimetric analysis was used to study the mass decay of biomass samples as a function of temperature and steam-to-carbon and CO_2/C ratios. Many of the woods showed self-similar profiles, and both the grasses and woods exhibited initial mass loss due to devolatilization, decomposition, and finally char burnout. As with the gasification of other hydrocarbon fuels, biomass yields a producer gas consisting mainly of CO_2, H_2O, CO, H_2, and CH_4. Other gaseous products of significance include formaldehyde, furan derivatives, phenols, and acetone.[24,25] These are at much lower concentrations and may not be detectable since the evolved gas species that are observed and their concentrations are highly dependent on the particular lignocellulosic composition of the biomass being gasified.

Figure 2 shows the mass decomposition of four representative biomass samples: oak, sugar maple, Douglas fir, and alfalfa. The greatest fraction of mass loss occurs during the pyrolysis stage between 300−400 °C when the biomass structural components are undergoing depolymerization and condensation reactions. Decomposition and carbonization of the remaining char structure continues during gasification. This is followed by high-temperature combustion reactions occurring as the oxygen contained in the fuel and brought in by the steam aid in burnout of the char structure between 700−850 °C. Two distinct regimes can be identified whose transition occurs at ∼400 °C. At this point, the biomass samples have been thermally processed to produce a more densified high-energy char. The samples all underwent a slow heating rate of 10 °C/min, and their mass burnout to residual ash fraction was completed by 950 °C.

The mass decay curve shows that biomass samples having a lower lignin content (alfalfa, cordgrass, and maple bark) yield a higher gasification mass percent residue. A similar observation was made when the fuels were completely combusted in a furnace during a separate test. When the pine needles sample was combusted, it similarly resulted in a high mass percent residue, though pine needles contain an extremely high (35% weight dry basis) composition fraction of lignin. Grasses, bark, and pine needles have a high mineral content that is observed in the burned mass combustion residue of the furnace crucible. Mineral content rather than lignin fraction appeared to be responsible for the percent combustion residue. When the TGA furnace was opened following pyrolysis (T < 400 °C) without gasification, only the grasses and barks that are low in lignin were observed to produce smaller volumes of char, which were between 20 and 30% less by weight. Lignin fraction rather than mineral content appeared to be responsible for the percent pyrolysis residue. This distinction was most notable for runs with no CO_2 recycle.

The scanning electron microscope with energy dispersion X-ray spectroscopy capability of the Materials Research Science and Engineering Center at Columbia was used to study several combusted, gasified, and unburned biomass samples to determine the presence of various elements on a weight % and atomic % basis. The spectrum reports were generated using Princeton-Gamma Tech software using beam energies of 5−15 KeV. Significant amounts of Cl, K, and Ca were observed for the alfalfa sample at 10 KeV beam energy. The gasification residue of alfalfa was found to be in excess of 40% K_2O by weight (Phyllis database[26] reports 44.2 ash weight %). Potassium gave the strongest signal in the energy-dispersive X-ray (EDX) spectra.

A comparison between the raw pulverized and steam-gasified samples of beachgrass having no CO_2 recycle appears in Table 1. The samples studied using the SEM with EDX yielded several significant differences. The gasification char pancake contained much lower weight percents of C and O, but the greatest fraction changes were due to mineral composition of the char. Ca rose from 2.45 to 14.25%, K from 4.99 to 27.23%, Fe from 6.23 to 15.35%, Si from 0.61 to 8.79%, and P from 1.31 to 8.69%. These increases in concentration likely led to an embrittlement of the quartz furnace and support rods during the testing as reported by Butterman and Castaldi.[27]

Senneca[13] studied the CO_2 enhanced steam gasification of biomass chars and found that the high char reactivity was more closely related to mineral composition and catalytic effects, particularly K_2O levels in the woods and residues, while the char-combustion and gasification rates were more closely related

Table 1. SEM/EDX of Biomass Elemental Analysis by Weight %

sample	C	O	Mg	P	Si	Fe	Na	K	S	Al	Cl	Ca
unburned maple bark	94.00	2.30	0.18	0.58	0.47	0.00	0.04	0.79	0.79	0.24	0.59	0.00
combusted maple bark	63.94	13.58	13.46	3.54	1.51	0.00	0.00	0.53	1.98	0.00	1.46	0.00
unburned poplar	91.91	5.84	0.08	0.29	0.27	0.00	0.00	0.99	0.31	0.32	0.00	0.00
combusted poplar	57.82	11.14	20.75	6.85	0.52	0.00	0.00	2.16	0.76	0.00	0.00	0.00
alfalfa leaf	79.13	8.70	0.78	0.88	0.19	0.00	0.37	5.29	0.75	0.00	1.14	2.77
alfalfa stalk	78.47	8.74	0.65	0.31	0.49	0.00	0.00	3.26	0.60	0.00	2.60	4.88
pulverized Douglas fir	95.96	0.00	0.00	0.02	0.00	0.87	0.00	0.89	0.47	0.28	0.40	0.54
gasified Douglas fir with 0% CO_2	91.25	7.15	0.13	0.11	0.00	0.00	0.00	0.04	0.26	0.68	0.26	0.11
pulverized beachgrass	77.19	2.22	0.27	1.31	0.61	6.23	0.00	4.99	0.63	0.00	2.15	2.45
gasified beachgrass with 0% CO_2	22.74	0.00	1.83	8.69	8.79	15.35	0.90	27.23	0.05	0.00	0.17	14.25
gasification furnace residue	0.00	17.84	0.20	0.00	81.10	0.00	0.05	0.44	0.01	0.00	0.31	0.06

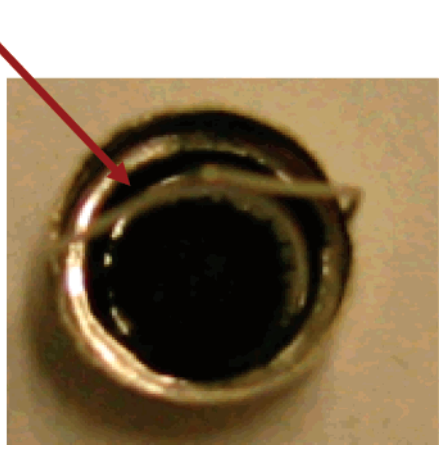

Figure 3. Large black char residue from 0% Douglas fir steam gasification.

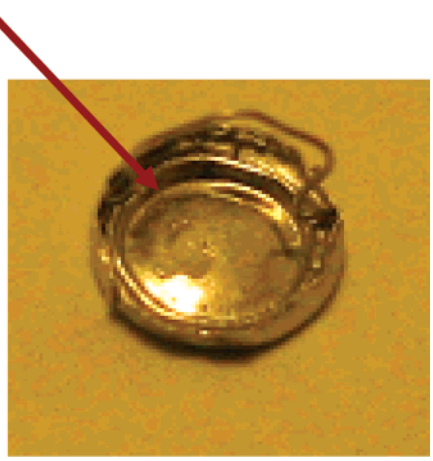

Figure 4. Light mineral residue film from 30% Douglas fir steam gasification.

to char pore structure. Biomass char having a highly porous network offers more sites for CO_2, H_2O, and O_2 adsorption. We also observed this correlation between gasification rate and porosity, as measured by the relative volume and mass of the gasification char. Analogous to the observation of biomass chars from Senneca, we also observed high K and Ca content in the steam-gasified chars of beachgrass.

Introducing CO_2 into the flow stream resulted in a markedly different biomass char burnout as evidenced in Figures 3 and 4. Enhanced char burnout was observed for all CO_2 recycle rates with complete char burnout for all tests using at least 30% CO_2 recycle. With no CO_2 introduced into the feed, a large black char residue was observed as in Figure 3 from 0% Douglas fir steam gasification. A distinctly different residue appears in Figure 4 from 30% Douglas fir, showing a light mineral residue film. This observation was consistent for all tests done with CO_2 injection in the feed.

For the beachgrass test sample, a much smaller char pancake resulted when there was 0% CO_2, and the black char looked significantly different since it was coated with a white mineral layer that the SEM/EDX analysis determined to be mostly K, Ca, and Fe. The lignin compositions of beachgrass (12%) and alfalfa (14%) are much lower than those of Douglas fir (28%) and poplar (24%), and the grasses show a characteristically smaller char pancake than the woods, corresponding to their lower lignin contents. This observation that low lignin herbaceous feedstocks generate smaller char residues as compared to those produced from high lignin woody feedstocks has been reported by other investigators. A similar correlation between

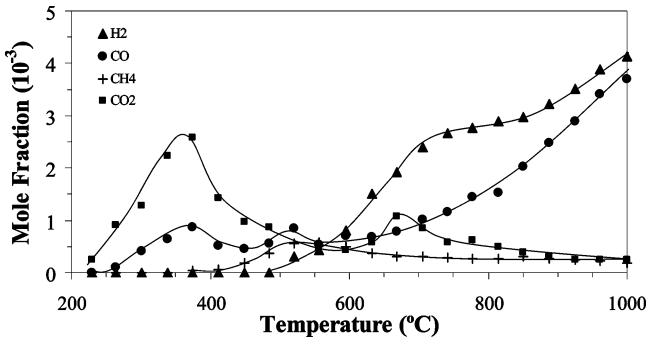

Figure 5. Gas evolution from green pine needles (0% CO_2).

high lignin content and large-volume pyrolysis char was observed by Demirbas[16] and Orfao et al.[17] Kawamoto and Saka[28] developed a mechanism for cellulose pyrolysis and found that the major pathway that feeds the pyrolysis products into the gasification reactions is the formation of levoglucosan. This molecule can be either broken down into low molecular weight products with a more complete gaseous evolution or polymerized to form polysaccharides that undergo surface carbonization with high levels of char in the absence of sufficient O or CO. A comparison of the gasification residues that appear in Figures 3 and 4 for 0% and 30% CO_2 shows the polysaccharide carbonization in the absence of sufficient O vs the mineral ash residue and the greater volatilization with the availability of sufficient O because of the CO_2 introduced.

3.2. Product Gas Evolution. A typical gas evolution plot showing the distribution of the four gases that were monitored (H_2, CO, CH_4, and CO_2) is shown in Figure 5. It represents the composite for pulverized green pine needles with no CO_2 injection. This sample has representative peaks characteristic of both lignin and cellulose decomposition because of its similar lignin (35%), cellulose (43%), and hemicellulose (22%) dry weight percent compositions. The gaseous evolution from brown dried pine needles was measurably different from green dried pine needles, indicating that chemical degradation of the biomass structural components occurring over time can effect the evolution profiles or the fraction of each species in the gasification product. Nevertheless, all of the profiles for woods, grasses, bark, and needles showed two distinct gas evolution regimes with a transition temperature in the neighborhood of 400 °C. At temperatures above 250 °C, when radical reactions become significant, CH_3 and H radicals formed from H abstraction and β-carbon scission reactions can begin to form CH_4, while at temperatures above 250 but below 400 °C, a lignin β-aryl phenolic elimination mechanism proposed by Kawamoto and Saka[28] results in the release of OH radicals. These OH radicals combine with available CO to produce CO_2 and generate new H radicals. This accounts for the low levels of CH_4 just prior to 400 °C and the spike in CO_2 for the gas evolution without CO_2 recycle for pulverized green pine needles. Alternative pathways for lignin degradation proposed by Kawamoto and Saka that become available at ~400 °C involve β-aryl and β-ether nonphenolic cleavage without the production of OH radicals that consume the CO needed for the methanation reactions. This would permit high levels of CO at the transition between thermal regimes at 400 °C, which is what we are seeing, and an increase in CH_4 concentrations after ~400−450 °C.

The rise in CO_2 and CO in the vicinity of 350−450 °C can also be attributed to several pathways involved in the slow pyrolysis of cellulose. Possible mechanisms involving depolymerization reactions converting the active cellulose to tar, char, and CO_2 via slow reactions are discussed by Banyasz et al.,[31]

and those involving decomposition of levoglucosan to volatile low molecular weight products or polymerization reactions to polysaccharides with release of CO and CO_2 and formation of a carbonized layer are discussed by Kawamoto et al.[32] The breakdown of levoglucosan in this transition-temperature interval may also follow a pathway involving the release of CH_3 radicals and CO from the methylglyoxal and glyceraldehyde intermediaries. These may be partially responsible for the peak in CO and the rise in CH_4 during this temperature interval.

This explanation is consistent with the observations in Figures 5 and 10. The concentrations of H_2 and CO are greatest at high furnace temperatures, while CH_4 levels are low throughout the gasification process and tend to decrease after 550 °C. Jangsawang and co-workers,[29,30] in examining the volatile product concentrations from the steam gasification of cellulose, noticed that H_2 and CO concentrations were very low below 540 °C. They observed an increasing H_2 concentration between 540 and 930 °C. A limiting temperature of ~930 °C was identified at which the production rate of H_2 and CO concentrations began to decline. They attributed the drop in H_2 production as being due to the competing processes of H_2 production from the gasification of the biomass and H_2 destruction resulting from molecular dissociation reactions becoming significant at temperatures of ~1000 °C. With no CO_2 recycle, there always remains a black char residue in the pan that can enter into the high-temperature gasification reactions, whereas with as little as 10% CO_2 recycle, nearly all of the biomass is exhausted before 950 °C. There exists no rapid drop in CO or H_2 concentrations at 0% CO_2. In Figures 6−9, this rapid decline in CO and H_2 concentrations at high percent CO_2 recycle rates represents the exhaustion of the biomass sample.

The collection of reactions describing the degradation of lignocellulosic structural material involve coupled mechanisms for which both molecular species and radical intermediates play significant roles. Additionally, reaction rates and product selectivity are influenced by the catalytic effect of the biomass mineral impurities. Gasification kinetics in the 500−1000 °C temperature range is controlled by many free radical reactions. Initiation reactions subsequent to the drying process become significant above 200 °C. This corresponds to the transition temperature at which mass decomposition becomes significant. Initial biomass decomposition reactions produce 2−6 carbon chain fragments or 5−6 carbon ring structures as well as many oxygenated species characteristic of the 5- and 6-carbon sugars in the cellulosic structures and the highly cross-linked aromatic phenylpropanoid composition of the lignin structural component. Typical of hydrocarbon thermal treatment whether by pyrolysis, gasification, or combustion, H abstraction and β-carbon bond scission play a significant role. Removal of OH radicals from cellulose and CH_3 radicals from lignin are also important radical reactions that continuously feed into the coupled mechanisms during the course of decomposition.

The thermal treatment of biomass fuels results in the evolution of gases typically found in hydrocarbon pyrolysis and gasification. Many of the reactions are similar, but the complex chemical structure of lignocellulosic material results in additional oxygenated species as well as aliphatic and aromatic compounds not ordinarily associated with hydrocarbon thermal decomposition.

During steam gasification at elevated temperatures (>700 °C), the concentration of CO increases with temperature due to the Boudouard reaction, which is endothermic.

$$C + CO_2 \rightarrow 2CO \qquad \Delta H = +172.5\ \text{kJ/mol} \qquad (6)$$

As gasification proceeds, CO_2 available in the flow combines with residual solid carbon in the sample carrier to produce increasing concentrations of CO. The CO evolution enhancement with increasing rates of CO_2/C appears in Figure 6 for beachgrass (S/C = 18) and in Figure 7 for poplar (S/C = 21). As the pyrolysis char is continually heated, the residual carbonyl groups are decarboxylated to CO and CO_2. Banyasz et al.[31] suggested that, while the fast high-temperature pyrolysis of cellulose (similar to their kinetic study) involves a mechanism whose pathways lead to the formation of formaldehyde, hydroxyacetaldehyde, CO, and CO_2, the slow low-temperature pyrolysis of cellulose (similar to our current investigation) involves formation of char, tar, CO_2, H_2O, and low-molecular-weight volatiles (particularly aldehydes) that are responsible for CO formation arising out of the biomass in the absence of CO_2 injection and occurring at low temperatures where the Boudouard reaction is not significant. Only at high gasification temperatures (>700 °C) are the Boudouard and steam-gasification reactions responsible for the CO levels observed.

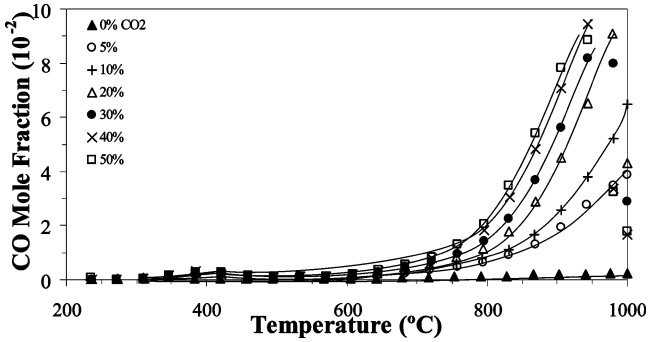

Figure 6. CO evolution from beachgrass (S/C = 18).

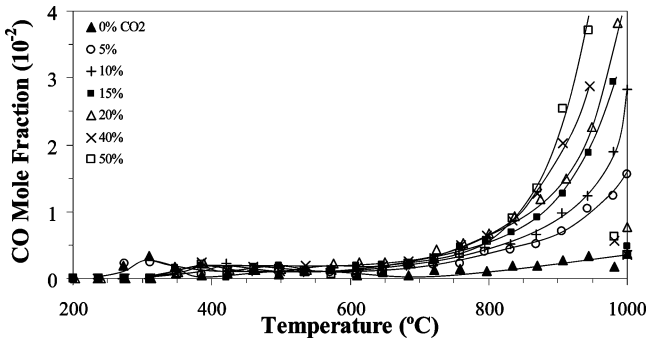

Figure 7. CO evolution from poplar (S/C = 21).

The highly reactive pyrolysis chars adsorb any available oxygen either brought into the gasifier as CO_2 or H_2O feed or arising out of the biomass material itself. They similarly adsorb any CO available, and this is released by subsequent heating of the char during gasification. As the residual char-adsorbed CO is liberated with increasing temperature, a continual supply of CO is produced that can help account for the uniformly increasing CO concentrations above 450 °C that appear in Figures 6 and 7. Demirbas[25] and Kawamoto et al.[32] developed different mechanisms for lignin decomposition that both include carbonization and CO gaseous evolution about 400 °C and are consistent with the observations in Figures 6 and 7. Cellulose pyrolysis initially involves the cleavage of OH radicals from the cellulose chain that subsequently react with CO in the gasifier to form CO_2 and H radicals. The CO_2 can be fed into the Boudouard reaction to augment CO concentrations at higher temperatures. The rapid drop in CO evolution appearing at the higher CO_2 recycle rates (20%, 30%, 40%, and 50%) above 950 °C represents the absence of carbon to feed into the Boudouard reaction.

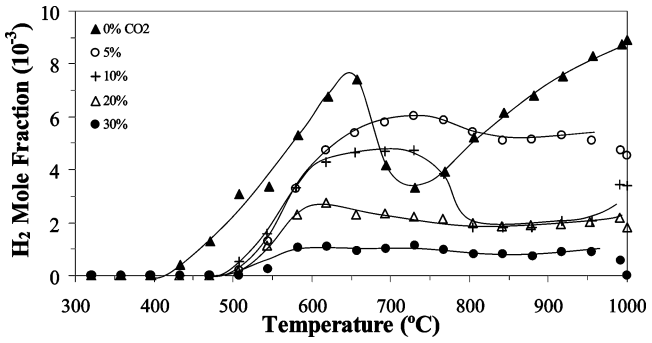

Figure 8. H_2 evolution from large sample beachgrass (S/C = 5.5). H_2 depression with CO_2 at $T > 750$ °C.

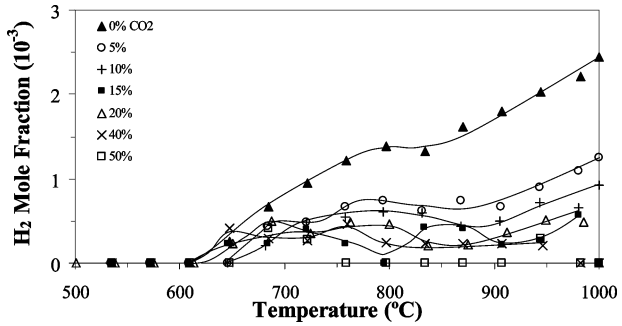

Figure 9. H_2 evolution from poplar (S/C = 21). H_2 depression with CO_2 at $T > 750$ °C.

Another significant reaction occurring during gasification (>550 °C) is the reforming reaction driven by relatively high CO_2 and H_2O concentrations compared to CO and H_2

$$C + H_2O \rightarrow CO + H_2 \qquad \Delta H = +131.3 \text{ kJ/mol} \quad (7)$$

This gasification reaction is responsible for the steep rise in H_2 concentration with temperature, as seen in Figure 8 for beachgrass (S/C = 5.5) and in Figure 9 for poplar (S/C = 21). The H_2 evolution depression with increasing rates of CO_2/C can be clearly observed for both the grass and wood samples. While the CO signal was the strongest and the enhancement was observed for all biomass feedstocks studied, only the lower steam-to-carbon ratios representing the higher carbon content tests for a given steam input rate gave a strong H_2 depression signal. H_2 production is favored at high gasification temperatures, but above 1000 °C, the competing rates of increasing dissociation to increasing formation of molecular H_2 result in a net decrease in the H_2 concentration in the dry gasification product stream. The H_2 depression due to higher CO_2 input rates appears to be due to a reverse shift in the highly endothermic steam-gasification reaction. This could be driven by the high concentrations of CO generated by a cluster of reactions that include the Boudouard reaction and the char-burnout reaction due to oxygen evolution from the biomass structure

$$C + {}^1/_2O_2 \text{ (from biomass structure)} \rightarrow CO \qquad \Delta H = -110.5 \text{ kJ/mol} \quad (8)$$

as well as O adsorption by the highly reactive char and CO desorption at the higher gasification temperatures.

The steam-gasification reaction couples with the water gas shift reaction and dominates between 500−600 °C,

$$CO + H_2O \rightarrow H_2 + CO_2 \qquad \Delta H = -41.2 \text{ kJ/mol} \quad (9)$$

to result in increasing H_2 concentrations in this temperature range. The reverse water gas shift reaction is favored at higher temperatures and, in combination with the Boudouard and char-burnout reactions and CO desorption from the char, presents a driving force for the reverse steam-gasification with a resultant decrease in H_2 concentration with increasing CO_2 recycle rate that should become more pronounced above 700 °C. This is what is observed in Figures 8 and 9 for H_2 depression as the CO_2 /C ratio is increased. Between 700−1100 °C, H radicals combine to give molecular H_2. Above 1100 °C, molecular H_2 breaks down, resulting in decreased H_2 yield at very high gasification temperatures. Dehydrogenation reactions are continuously occurring during the biomass decomposition and devolatilization. The absence of H_2 evolution at detectable concentrations can be explained by the Demirbas[25] mechanism that involves a biomass free radical stabilized by the addition of H abstracted from either a donor molecule or a high molecular weight fraction. Biomass having high cellulosic content degrades sooner, no longer needing H consumption for stabilization, and it shows an earlier mass decomposition and a H_2 evolution rise sooner than lignitic material. This is experimentally verified in our mass decay curve in which the grasses with lower lignin content decompose earlier. We also see evidence for the credibility of this mechanism in the H_2 evolution from poplar with higher lignin content occurring later, ∼600 °C in Figure 9, as compared to beachgrass with lower lignin content occurring earlier at ∼400 °C in Figure 8.

Methane evolution occurs at low levels throughout the gasification process, but a sharp rise in methane formation observed in both the woods and the grasses between 300−450 °C is due to methyl and methoxy radical reactions particular to the lignocellulosic composition and the molecular methanation reactions

$$2CO + 2H_2 \rightarrow CH_4 + CO_2 \qquad \Delta H = -246.9 \text{ kJ/mol} \quad (10)$$

$$CO + 3H_2 \rightarrow CH_4 + H_2O \qquad \Delta H = -205.7 \text{ kJ/mol} \quad (11)$$

$$C + 2H_2 \rightarrow CH_4 \qquad \Delta H = -74.4 \text{ kJ/mol} \quad (12)$$

Steam introduced in the feed for gasification along with the CO available in the furnace combine via the water gas shift reaction to produce the H_2 available for reaction during pyrolysis. This H_2 is consumed through direct hydrogenation to yield a continual supply of methane. In the neighborhood of 400 °C, at the transition between regimes at which the H_2 and CO concentration levels rise, a corresponding increase in CH_4 evolution can be seen. The Demirbas[25] mechanism for lignin decomposition, whose rate is greatest between 350−500 °C, involves guaiacol derived from thermal cracking of the phenylpropane units of the lignin lattice. Guaiacol undergoes thermal cleavage to pyrocatechol and the methyl radical or a phenol cresol and the methoxy radical. The methoxy radical abstracts H from guaiacol to form methane, resulting in an increased concentration of CH_4. This peak production of methane between 400−600 °C appears in Figure 10.

The net effect of depressing H_2 production due to CO_2 injection that is observed to commence at ∼550−600 °C is to cause a concomitant CH_4 evolution depression commencing during the same temperature interval due to a decrease in H_2 available to feed into the methanation reactions. This methane evolution depression with CO_2 recycle appears in Figure 10 for beachgrass (S/C = 5.5). Since the steam input rate is constant

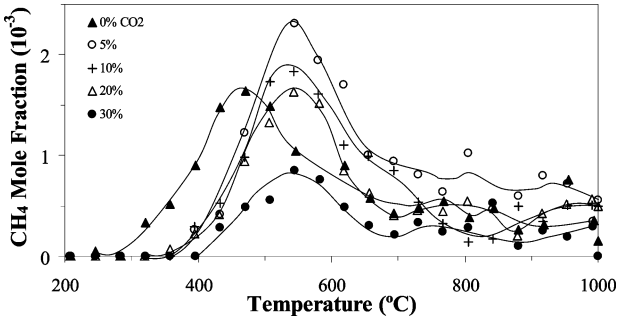

Figure 10. CH_4 evolution from large sample beachgrass (S/C = 5.5).

for all gasification runs, the larger mass samples correspond to lower S/C ratios.

The enhanced CO production and depressed H_2 production that we observed as a result of the introduction of CO_2 in the feed during biomass steam-gasification is analogous to the concentration changes observed by others during adsorption-enhanced reforming (AER) of a variety of hydrocarbon fuels using several different types of reactor configurations. Pfeifer et al.[9] observed enhanced char combustion through the internal recycle of CO_2, and less efficient removal of CO_2 led to higher levels of CO and lower levels of H_2 in the producer gas for the 600−700 °C temperature range studied. Iyer et al.[5] observed these changes as the adsorbent became saturated and the CO_2 levels began to rise in their fixed-bed reactor. Just before breakthrough, as CO_2 levels abruptly rose, CO conversion to CO_2 dropped, and a steep rise in CO and drop in H_2 concentrations were detected.

We also observed trends with CO_2 feed injection: enhanced CO and depressed H_2 production with increasing CO_2 feed concentrations. In addition, low steam-to-carbon ratios evidenced a greater sensitivity and a more pronounced effect on the gasification enhancement or depression. Similar CO enhancement and H_2 depression were observed by Alma et al.[8] in their AER study of steam gasifications of willow and switchgrass. At 650 °C with increasing adsorption of CO_2, conversion of CO to CO_2 from shifting (WGS) increased, and this led to decreased concentrations of CO in the batch reactor and simultaneously enhanced H_2 production associated with the CO_2 removal. The steam gasification of wood pellets in a fluidized bed using AER was investigated by Mollenstedt et al.[10] The product gas composition−tar concentration graph showed a rapid rise in CO_2 levels before breakthrough, corresponding to a similar rise in CO, a drop in H_2, and a continuous production of low levels of CH_4 throughout the run. Iyer et al.[4] observed a greater depression in the level of CO to CO_2 conversion and a lower level of H_2 production for lower S/CO ratios for the entire temperature interval 450−750 °C over which the WGS reaction dominates.

3.3. Comparison with ASPEN Simulation. As a confirmation of the effect of CO_2 injection on the steam gasification of a carbon based fuel, the current experimental observations were compared to the numerical results of an ASPEN simulation done by Castaldi and Dooher[23] for the steam gasification using CO_2 recycle. Using a stoichiometric mix of CO derived from the reformer product gases and O_2 brought in for combustion, the CO is catalytically combusted. Part of the energy from this exothermic combustion of CO is used to drive the endothermic gasification in the reformer. Steam, a recycled fraction of the CO_2 produced by the combustion process, and the pure carbon fuel are gasified, producing CH_4, CO, H_2, CO_2, and H_2O as products. The effect on H_2, CO, and CH_4 evolution was calculated for a variety of steam-to-carbon ratios (S/C) and

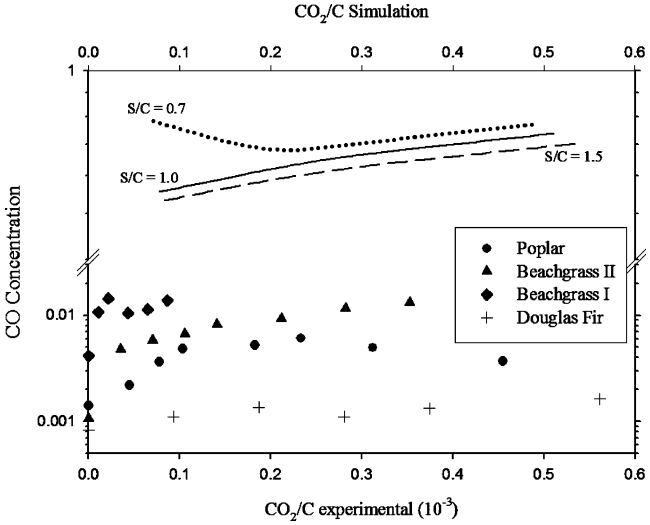

Figure 11. CO evolution enhancement with CO_2−Biomass experimental and simulation.

CO_2/C ratios. Though the S/C and CO_2/C ratios varied greatly between experimental and numerical conditions, the agreement in the general trends of enhancement or depression was excellent.

In order to compare the simulation results with those from the biomass gasification experiments, the species concentrations were calculated on a dry basis leaving the reformer. The recycle parameter was chosen to be (CO_2 in the feed)/(C in the feed) on a mole basis. The biomass graphs were plotted against the ratio of the CO_2 flow rate fed into the gasifier divided by the carbon rate of decay in the biomass. The decay rate of biomass was determined only for the high-temperature gasification regime as identified from the mass decay slope evaluated at ∼750 °C. This was calculated by measuring the slope of the mass decay curve for the particular biomass feedstock, using the constant temperature ramp rate of the thermal analyzer and a knowledge of the % carbon composition of the biomass molecular "formula" to determine the experimental CO_2/C ratio.

Figure 11 compares the experimental and numerical CO enhancements as a function of the ratio of CO_2/C. The calculation of the decomposition-rate slope was an average value representing the temperature interval of 700−900 °C for the mass decay curve of the particular biomass feedstock. At the higher CO_2/C ratios, the CO mole fraction on a dry basis was predicted by the simulation to increase for all CO_2/C ratios. This general rising trend is seen for all four experimental biomass feedstocks. The CO enhancement effect was predicted to be greater for lower S/C ratios. Numerical calculations of CO mole fractions show an increase as the S/C ratio decreased from 1.5 to 1.0 to 0.7. This numerical trend is again confirmed for all four biomass samples. The stronger enhancement for lower S/C ratios is seen for the two beachgrass samples with beachgrass I (S/C = 5.5) showing a more pronounced enhancement than that of beachgrass II (S/C = 18) or either of the two woods, poplar (S/C = 21) or Douglas fir (S/C = 48).

Figure 12 compares the H_2 evolution depression as observed experimentally and confirmed numerically by the ASPEN simulation. The H_2 mole fraction on a dry basis decreases monotonically for the higher values of CO_2/C, and the H_2 depression effect is more noticeable with decreasing S/C ratios. The simulation curve for S/C = 0.7 shows the greatest H_2 depression followed by that for S/C = 1.0 and then that for S/C = 1.5. H_2 depression can be clearly seen for the beachgrass I sample (S/C = 5.5), whose depression was most pronounced

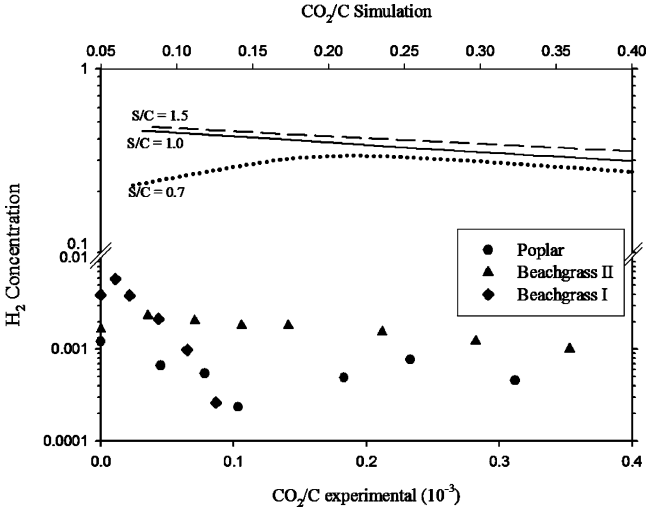

Figure 12. H_2 evolution depression with CO_2—Biomass experimental and simulation.

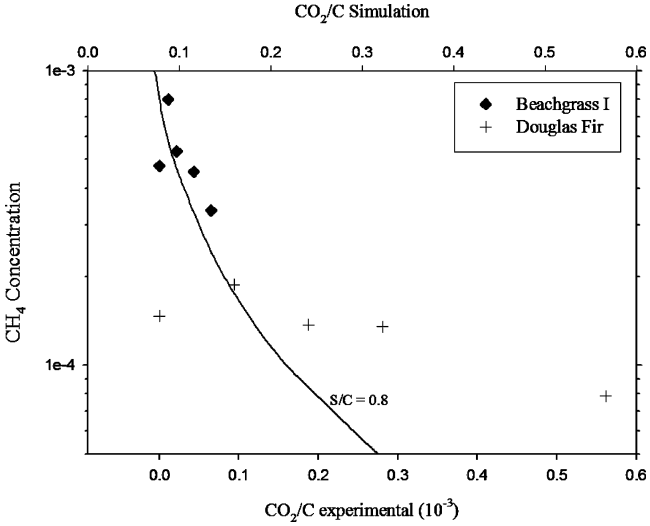

Figure 13. CH_4 evolution depression with CO_2—Biomass experimental and simulation.

when compared to those for beachgrass II (S/C = 18) or the wood sample poplar (S/C = 21). Similar findings for the H_2 depression with rising CO_2 and CO levels were observed by Iyer et al.[4] At lower S/CO ratios, they noticed that the drop in H_2 production was more pronounced and occurred earlier, indicating a greater sensitivity to the rise in CO_2 levels.

The ASPEN simulation was performed for a pure carbon feedstock that is significantly different from biomass, for which the complex lignocellulosic structure is a partially crystalline and partially highly branched and cross-linked aromatic with a significant number of oxygenated functional groups. The CO enhancement and H_2 depression trends common to both were observed at the higher gasification temperatures in which the two main reactions controlling the thermal degradation were the steam reforming and the Boudouard reactions. At these temperatures, the biomass char is essentially a condensed carbon skeleton with mineral impurities that will exert a catalytic effect on the reactivity of the char but not significantly alter the concentrations of products from the high-temperature gasification reactions.

Saturated steam is fed into the line at atmospheric pressure, while CO_2 is fed in at much higher levels of 5−50% mole fraction. The high levels of CO_2 compete for adsorption sites on the gasification char. Every mole of CO_2 that reacts with the carbon in the biomass produces two moles of CO via the Boudouard reaction. High levels of CO are a negative driving force for the steam-gasification reaction and result in lower levels of H_2 production. Higher levels of CO_2 and lower levels of H_2O favor increased levels of CO and decreased levels of H_2, hence resulting in the enhanced CO and depressed H_2 production in steam reforming of a carbon based feedstock using CO_2 to enhance the gasification process.

Finally, Figure 13 shows the CH_4 evolution depression that was clearly discernible in some of the biomass graphs and the corresponding CH_4 evolution depression with CO_2 as predicted by the ASPEN simulation. For a given S/C = 0.8, with increasing CO_2/C ratio as the fraction of CO_2 brought back into the reformer (gasifier) increases, the CH_4 mole fraction coming out of the gasifier on a dry basis decreases. This simulation trend is confirmed experimentally in Figure 13. A general decrease in CH_4 evolution with increasing $\%CO_2$ can be observed for both the wood Douglas fir sample (S/C = 48) and a more pronounced CH_4 depression with CO_2 for beachgrass I (S/C = 5.5). These experimental CH_4 evolution levels were taken at 750 °C, at which temperature H_2 was experiencing a decline. CH_4 production is not favored at these higher gasification temperatures. Both radical and molecular methanation reactions involve hydrogenation for CH_4 formation. At the higher gasification temperatures where we are observing H_2 depression with increasing CO_2/C ratios and decreasing S/C ratios, we can expect a depression in CH_4 due to the decreased levels of H_2 available. All of the methanation reactions that involve the direct hydrogenation of carbon in the char require two or more moles of molecular H_2 for the production of each mole of CH_4. Therefore, a much larger depression in H_2 corresponds to the decrease in CH_4 levels that we are observing, and we could expect less sensitivity in CH_4 depression as a function of CO_2/C ratio. This difference in behavior can be seen when comparing Figures 12 and 13.

4. Conclusion

A series of steam-gasification tests were performed using a variety of wood and grass samples in which varying concentrations of CO_2 were introduced to study the influence of CO_2 on the steam-gasification products of biomass. Both mass decomposition and gas evolution exhibited two regimes that had a transition in the vicinity of 400 °C. The bulk of the biomass decomposition occurred between 300−400 °C and was completed by 950 °C. Those biomass samples with lower-lignin fractions (beachgrass, maple bark, and alfalfa) were observed to yield higher mass % gasification residues but smaller pyrolysis char volumes when compared to the higher-lignin feedstocks (oak, sugar maple, pine, Douglas fir, and pine needles). Large gasification residues correlated well with high mineral content, whereas large pyrolysis char residues correlated well with high lignin content contained in the biomass. Introduction of CO_2 into the line reduced the volume of gasification residue as observed by the presence of a smaller char volume or ash residual in the sample carrier.

CO production becomes significant above 600 °C when the Boudouard, steam-gasification, reverse WGS, and char-combustion reactions all favor the increase in CO concentration with temperature. The H_2 concentration does not become measurable until 400 °C for beachgrass and 600 °C for poplar with H radical addition and steam gasification being responsible for rising H_2 levels at elevated temperatures. While methane production is low for all temperatures during the steam-gasification process,

a distinct increase in rate occurs between 300−550 °C. The highly exothermic methanation reactions between the CO present and the H_2 being formed by the WGS reaction in this temperature interval, in addition to nonphenolic cleavage mechanisms for lignin degradation, are responsible for the increase in methane production. The OH radical is produced by both lignin and cellulose decomposition, and the reaction of the OH radical with CO is a significant propagation reaction producing H radicals while consuming CO that could otherwise enter the methanation or WGS reaction. The α-ether, *β*-aryl, and *β*-ether nonphenolic cleavage pathways without OH radical formation that can account for the rise in CO production between 350−400 °C also involve the phenoxy radicals not undergoing coupling at the higher temperatures above 450 °C but instead releasing CH_3 by cleavage of the C−O bond in the methoxy group. This can help explain the strong methane peaks we observed between 450−550 °C.

Addition of CO_2 into the feed was observed to significantly enhance the CO evolution above 700 °C, depress the H_2 concentration above 600 °C, and, at high CO_2 concentrations, depress the CH_4 levels above 700 °C. Higher CO_2 concentrations and lower S/C ratios led to more pronounced enhancement or depression. The trends for CO enhancement and H_2 and CH_4 depression with increasing CO_2 concentration introduced were confirmed by the ASPEN simulations. The CO enhancement and H_2 depression were more pronounced for the lower S/C ratios for CO, H_2, and CH_4, particularly at the higher CO_2/C ratios that were more characteristic of the experimental values. The simulation is for the CO_2 enhanced steam gasification of a carbon fuel rather than the more complex lignocellulosic biomass fuel. Our recycle parameter CO_2/C fed into reformer used for simulation comparisons is based on the analogous carbon mass decay rate calculated experimentally for each fuel at ∼750 °C rather than at a constant operating temperature of 1000 °C as in the catalytically controlled reaction gasifier (CCRG) process. The range in S/C ratios was from 0.7 to 1.5 for the numerical runs and from 5.5 to 48 for the experimental runs. Though the parameters differed in value, all of the trends in enhancement and depression due to CO_2 injection as well as the sensitivity to S/C ratio showed similar behavior and there was excellent correlation between the numerical ASPEN simulations and the experimental biomass observations.

Literature Cited

(1) International Energy Agency. *World Energy Outlook—Renewable Energy*; International Energy Agency: Paris, 2007; Chapter 7.

(2) Energy Information Administration. *Annual Energy Review*; Energy Information Administration: Washington, DC, 2006.

(3) U.S. Department of Energy. *Biomass as Feedstock for a Bioenergy and Bioproducts Industry: The Technical Feasibility of a Billion-Ton Annual Supply*; EERC Biomass Program Feasibility Study; U.S. Department of Energy: Washington, DC, April 2005.

(4) Iyer, M.; Ramkumar, S.; Fan, L. S. High Purity H_2 Production with in-situ CO_2 and Sulfur Capture. *AIChE Annu. Conf.* **2006**.

(5) Iyer, M.; Ramkumar, S.; Fan, L. S. *Enhanced H_2 Production Integrated with CO_2 Separation in a Single-Stage*; DOE Annual Report, Contract No. DE-FC26-03NT41853; U.S. Department of Energy: Washington, DC, Oct 2006.

(6) Bretado, M. E.; Collins-Martinez, V.; Lopez-Ortiz, A. Thermodynamic Analysis for the Absorption-Enhanced Water Gas Shift Reaction (AEWGS) for the Production of Hydrogen. *AIChE Annu. Conf.* **2006**.

(7) Specht, M.; Bandi, A.; Baumgart, F.; Moellenstedt, T.; Textor, O. Enhanced Reforming Reaction for Hydrogen Production from Carbonaceous Feedstock. In *Hydrogen Energy Progress XIII*, Proceedings 13th World Hydrogen Energy Conference, Beijing, China, 2000; Mao, Z. Q., Veziroglu, T. N., Eds.; International Association for Hydrogen Energy: Miami, FL, 2000; p 1203.

(8) Alma, M. H.; Cinar, O.; Oz, H. R. Zero-Emission Method for Hydrogen Production. Presented at International Hydrogen Energy Congress and Exhibition, Istanbul, Turkey, July 2005.

(9) Pfeifer, C.; Proll, T.; Puchner, B.; Hofbauer, H. H_2-Rich Syngas From Renewable Sources By Dual Fluidized Bed Steam Gasification of Solid Biomass. Presented at 12th International Conference on Fluidization, Vancouver, Canada, 2007; Vol. RP4, Article 109.

(10) Mollenstedt, T. M.; Sichler, P.; Specht, M.; Michel, M.; Berger, R.; Hein, K. R. G.; Hoftberger, E.; Rauch, R.; Hofbauer, H. *New Approach for Biomass Gasification to Hydrogen*; Center for Solar Energy and Hydrogen Research Publications: Austria, 2004; http://members.aon.at/biomasse/aer_rom.pdf.

(11) Song, C. Overview of Hydrogen Production Options for Hydrogen Energy Development, Fuel-Cell Fuel Processing and Mitigation of CO_2 Emissions. Proceedings of 20th International Pittsburgh Coal Conference, Pittsburgh, PA, Sept 2003.

(12) Nehrozoglu, A.; Foster Wheeler Power Group Inc. *Advanced CO_2 Cycle Power Generation*; Technical Progress Report, U.S. DOE Contract: DE-FC26-02NT41621; U.S. Department of Energy: Washington, DC, Jan 2004.

(13) Senneca, O. Kinetics of pyrolysis, combustion and gasification of three biomass fuels. *Fuel Process. Technol.* **2007**, *88*, 87.

(14) Minkova, V.; Marinov, S. P.; Zanzi, R.; Bjornbom, E.; Budinova, T.; Stefanova, M. L.; Lakov, L. Thermochemical treatment of biomass in a flow of steam or in a mixture of steam and carbon dioxide. *Fuel Process. Technol.* **2000**, *62*, 45.

(15) Ye, D. P.; Agnew, J. B.; Zhang, D. K. Gasification of a South Australian low-rank coal with carbon dioxide and steam: Kinetics and reactivity studies. *Fuel* **1998**, *77*, 1209.

(16) Demirbas, A. Production and Characterization of Bio-Chars from Biomass via Pyrolysis. *Energy Sources, Part A* **2006**, *28*, 413.

(17) Orfao, J. J. M.; Antunes, F. J. A.; Figueiredo, J. L. Pyrolysis kinetics of lignocellulosic materials—Three independent reactions model. *Fuel* **1999**, *78*, 349.

(18) Babu, B. V.; Chaurasia, A. S. Modeling, simulation and estimation of optimum parameters in pyrolysis of biomass. *Energy Convers. Manage.* **2003**, *44*, 2135.

(19) Sheth, P. N.; Babu, B. V. Effect of Moisture Content on Composition Profiles of Producer Gas in Downdraft Biomass Gasifier. Presented at 2nd International Congress on Chemistry and the Environment (ICCE), Indore, India, Dec 2005.

(20) Sears, J. T.; Muralidhara, H. S; Wen, C. Y. Reactivity Correlation for the Coal Char−CO_2 Reaction. *Ind. Eng. Chem. Process Des. Dev.* **1980**, *19*, 358.

(21) Ochoa, J.; Cassanello, M. C.; Bonelli, P. R; Cukierman, A. L. CO_2 gasification of Argentinian coal chars: A kinetic characterization. *Fuel Process. Technol.* **2001**, *74*, 161.

(22) Messenbock, R. C.; Dugwell, D. R.; Kandiyoti, R. CO_2 and steam-gasification in a high-pressure wire-mesh reactor: The reactivity of Daw Mill coal and combustion reactivity of its chars. *Fuel* **1999**, *78*, 781.

(23) Castaldi, M. J.; Dooher, J. P. Investigation into a Catalytically Controlled Reaction Gasifier (CCRG) for Coal to Hydrogen. *Int. J. Hydrogen Energy* **2007**, in press; doi: 10.1016/j.ijhydene.2007.06.014.

(24) Marques, A. V.; Pereira, H.; Rodrigues, J.; Meier, D.; Faix, O. Isolation and comparative characterization of a Bjorkman lignin from the saponified cork of Douglas fir bark. *J. Anal. Appl. Pyrolysis* **2006**, *77*, 169.

(25) Demirbas, A. Mechanisms of liquefaction and pyrolysis reactions of biomass. *J. Energy Convers. Manage.* **2000**, *41*, 633.

(26) The Phyllis biomass database of the Energy Research Center of the Netherlands; www.ecn.nl/phyllis/ (accessed 2007).

(27) Butterman, H. C.; Castaldi, M. J. Hydrogen Production via Gasification of Biomass Fuels. Presented at 26th International Conference on Incineration and Thermal Treatment Technologies (IT3), Phoenix, AZ, May 2007.

(28) Kawamoto, H.; Saka, S. Wood pyrolysis mechanism on molecular basis for selective conversion into liquid fuels. Presented at Sustainable Energy and Environment, Thailand, Nov 2006.

(29) Jangsawang, W.; Gupta, A. K.; Kitagawa, K.; Lee, S. C. High Temperature Steam and Air Gasification of Non-Woody Biomass Wastes. Presented at 2nd Joint International Conference on Sustainable Energy and Environment, Thailand, Nov 2006.

(30) Jangsawang, W.; Klimanek, A.; Gupta, A. K. Enhanced Yield of Hydrogen From Wastes Using High Temperature Steam Gasification. *J. Energy Res. Technol.* **2006**, *128* (3), 179.

(31) Banyasz, J. L.; Li, S.; Lyons-Hart, J.; Shafer, K. H. Gas evolution and the mechanism of cellulose pyrolysis. *Fuel* **2001**, *80*, 1757.

(32) Kawamoto, H.; Murayama, M.; Saka, S. Pyrolysis behavior of levoglucosan as an intermediate in cellulose pyrolysis: Polymerization into polysaccharide as a key reaction to carbonized product formation. *J. Wood Sci.* **2003**, *49*, 469.

(33) U.S. Dept. of Energy Biomass Program, Biomass Feedstock Composition and Property Database; http://www1.eere.energy.gov/biomass/feedstock_databases.html (accessed 2007).

(34) Biomass Energy Foundation: Proximate/Ultimate Analysis; http://www.woodgas.com/proximat.htm (accessed 2007).

(35) European Agriculture and Forestry Biomass Network; http://www.vtt.fi/virtual/afbnet/ (accessed 2007).

(36) Oak Ridge National Laboratory, Bioenergy Feedstock Development Programs; http://bioenergy.ornl.gov/papers/misc/biochar_factsheet.html (accessed 2007).

Received for review August 24, 2007
Revised manuscript received October 28, 2007
Accepted October 29, 2007

IE071160N